DEM Generation by Means of ERS Tandem Data

Giancarlo Rufino, Antonio Moccia, and Salvatore Esposito

Abstract—**This paper presents an application of the European Remote Sensing (ERS) satellites' radar data to digital elevation model (DEM) generation. The selected test site is the Sannio-Matese area in southern Italy, where several corner reflectors (CR's) were deployed to be used as ground control points (GCP's) for height measurement accuracy validation. First of all, an analysis of the CR response in radar images is presented. Then, the procedure for image pair geometric registration and interferogram formation is described in detail. A quantitative analysis is also performed by comparing these interferograms to the corresponding products obtained by using the ISAR software, officially distributed by the European Space Agency (ESA). Reported correlation values show that only tandem pairs allow an efficient interferometric processing to be performed, thanks to their short-time baseline (one day), whereas correlation adequate for differential interferometry could not be achieved. The method adopted for the computation of the interferometric baseline components on the basis of satellite orbital data is described, including the GCP-based corrections. The procedure was applied to obtain DEM's of a 10 × 10 km^2 subarea characterized by very high correlation coefficients (0.6). The best attained values of the GCP height measurement accuracy were about 4 m. Finally, the DEM's were compared, giving root mean square (rms) differences less than 20 m in the best case.**

Index Terms— **ERS-1/ERS-2 Tandem, orbital data, synthetic aperture radar (SAR) interferometry, terrain mapping.**

I. Introduction

SYNTHETIC aperture radar (SAR) interferometry has been proposed as a technique for high-resolution and high-accuracy topographic mapping [1], [2] as well as surface motion detection [3]. Among the proposed and existing spaceborne interferometric techniques, repeat-track interferometry has a significant advantage: it uses a single antenna that observes the same area from different orbits. This allows us to surpass complexity and cost problems connected to the simultaneous use of two spaceborne antennas, but it introduces new critical issues, mainly decorrelation consequent to the nonsimultaneous acquisition of the interferometric pair. Further limitations are connected to baseline uncertainty and variation and orbit selection for adequate coverage. The tandem operation of European Remote Sensing (ERS)-1 and ERS-2 satellites is the first space mission aimed at SAR interferometric coverage on a global scale and with a short temporal baseline. During tandem operation, the two satellites fly in the same orbital plane at the same mean altitude and the orbit phasing is adjusted to make ERS-2's ground track be coincident with that of ERS-1 24 h earlier. As a consequence, any point on the ground can be revisited after one day and reobserved in strip mode under identical conditions (altitude, incidence, local time, etc.) [4]. The availability of tandem data certainly deserves great interest because several authors have pointed out the need of spaceborne missions for global topographic mapping by means of SAR interferometry [5] and the problems connected to accurate digital elevation model (DEM) production when temporal decorrelation effects are significant [6], [7].

In the last few years, we have been studying the above aspects, focusing our interest also on ERS tandem data. In particular, the Consortium for Research on Advanced Remote Sensing Systems (CORISTA), Naples, Italy, was one of the investigators of the research "earthquakes prediction in tectonic active areas using space techniques" founded by the Commission of the European Communities. The responsibility of CORISTA was related to the detection of small crustal motions by means of space-based techniques (e.g., SAR interferometry and GPS) [8]. The area of interest was located in southern Italy (Sannio-Matese region, about 35 × 40 km^2, centered in 41°15′ N 14°25′ E) and was characterized by significant heterogeneous land use: wide agricultural extensions, forests, bare soils, urban and industrial sites, and lakes and river basins. Furthermore, the terrain elevation extended from 100 to 1100 m, including large flat areas and steep reliefs. Several corner reflectors (CR's) were deployed on the test area, to be used as reference targets for interferometry, by the research Co-Investigators, headed by Prof. P. Murino (Department of Space Science and Engineering, University of Naples). Although the use of a set of ground control points (GCP's) for height measurement accuracy assessment has some limitations, as pointed out in [9], this area certainly represents an interesting test bed for interferometric processing.

This paper describes the procedure we developed and applied to the Sannio-Matese area to produce DEM's starting from C-band single-look complex (SLC) tandem data acquired in strip mode. After selection of interferometric pairs by means of the baselines available at the European Space Agency (ESA)/ESRIN server, the procedure consists of CR identification, geometric registration of the pair, and interferogram production, phase unwrapping, and baseline estimation. Quantitative evaluations were performed by means of correlation analysis and DEM accuracy assessment. To this end, the "ISAR-Interferogram Generator" software, officially distributed by ESA, was applied to repeat the geometric registration for correlation validation, whereas, the CR's were used to refine baseline computation and as GCP's to check the height accuracy.

Manuscript received November 26, 1996; revised December 3, 1997.

G. Rufino and A. Moccia are with the Dipartimento di Scienza e Ingegneria dello Spazio "Luigi G. Napolitano," Università degli Studi di Napoli "Federico II," 80125 Napoli, Italy (e-mail: amoccia@unina.it).

S. Esposito is with Consorzio di Ricerca su Sistemi di Telesensori Avanzati, 80125 Napoli, Italy.

Publisher Item Identifier S 0196-2892(98)05628-9.

TABLE I
CR RADIOMETRIC ANALYSIS. SATISFACTORY VALUES FOR TEST-A ARE POSITIVE AND MUCH LESS THAN UNITY AND, FOR TEST-B ARE, SMALL AND NEGATIVE [10]. SATISFACTORY BROADENINGS ARE LESS THAN 20%. SATISFACTORY ISLR AND PSLR ARE LESS THAN −14 AND −17 dB, RESPECTIVELY [12]

Corner Reflector		test_A	test_B	Slant range			Azimuth		
no.	site			broad-ening	ISLR (dB)	PSLR (dB)	broad-ening	ISLR (dB)	PSLR (dB)
1	Formicola	0.14	-0.81	-1 %	-12	-20	16 %	-8	-16
2	Dragoni	0.13	-0.74	4 %	-9	-22	13 %	-11	-15
3	Letino	0.17	-0.75	14 %	-6	-25	15 %	-7	-19
4	Castelpizzuto	0.16	-0.60	2 %	-8	-17	10 %	-9	-18
5	Cantalupo	0.04	-0.75	11 %	-14	-25	12 %	-10	-22
6	Baranello	0.10	-0.71	16 %	-7	-19	20 %	-9	-19
7	Guardiaregia 1	0.18	-0.73	6 %	-6	-14	7 %	-8	-14
8	Guardiaregia 2	0.16	-0.81	1 %	-10	-20	13 %	-10	-37
9	Cerreto S.	0.18	-0.73	-2 %	-5	-15	12 %	-5	-14

TABLE II
PROCESSED ERS TANDEM DATA: FRAME 819, TRACK 129, QUADRANT 2

Tandem	ERS-1		ERS-2	
pair	orbit no.	date	orbit no.	date
1	21159	01 Ago 95	1486	02 Ago 95
2	22662	14 Nov 95	2989	15 Nov 95
3	24165	27 Feb 96	4492	28 Feb 96
4	24666	02 Apr 96	4993	03 Apr 96

II. CR DETECTION

The CR's were deployed over a very large area without following a particular geometric pattern in along or across-track direction. Furthermore, additional man-made point targets were present in the densely inhabited area. As a consequence, the CR's were not immediately identified in the available SLC images. Therefore, a thorough radiometric analysis was required. Starting from the knowledge of the CR geographic coordinates, the first step of the procedure consisted in the extraction of a small area, approximately centered in each corner, identified by visual inspection. Then the criteria proposed in [10] were applied to evaluate quantitatively the CR location. The best point targets were identified by means of two coefficients: test-A, related to the ratio between the background and the pixel amplitude, and test-B, a measure of the peak width. Since at this stage it was not yet possible to identify univocally all CR's, a more accurate analysis was carried out by computing the broadenings, the integrated sidelobe ratios (ISLR's) and the peak sidelobe ratios (PSLR's), both in range and azimuth directions [11]. Table I summarizes the overall results of the above procedure applied to the considered SLC images (Table II). Unfortunately, the radiometric quality was poor [12] and the number of satisfactory CR's was limited.

III. GEOMETRIC REGISTRATION AND INTERFEROGRAM PRODUCTION

The selected area for interferometric processing was a subset of a quadrant consisting of 9000 single-look azimuth pixels × 1900 single-look slant range pixels, including all of the nine CR's listed in Table I. A preliminary coarse registration at pixel accuracy of each interferometric pair was performed by means of a two-dimensional (2-D) rigid translation based on the previous localization of the nine CR's. Our procedure for fine registration [13] is based on the automatic identification of a large number of GCP's in addition to the already identified CR's. This task cannot be easily accomplished with SAR data covering large areas [14] and requires a careful strategy. To this end, each image was divided into 512 × 128 pixel subareas, and for each subset, the brightest point target was assumed as GCP. Subsequently, each subarea was ten times oversampled by means of cubic B-splines and the subpixel shifts between homologous areas were computed by using the cross correlation of the GCP amplitudes (Table III). Finally, the geometric registration was performed by means of bicubic polynomials, whose coefficients were computed with least-squares approximation, using as input the subpixel shifts (Table IV).

Shaded regions in Table III show decorrelated areas where the procedure was not able to find the shifts. This result will be verified also by the correlation analysis shown in the next paragraph. The range and azimuth shifts computed for the tandem pair 3 are quite regular (Table III-b). In particular, the azimuth shifts are nearly constant over the whole image, while the range shifts increase by approximately one pixel from near to far range. This is probably due to slight orbit misalignments and/or attitude differences. Furthermore, the two images were focused independently, each one with its Doppler centroid frequency and bandwidth varying from near to far range. Differently, the shifts of pair 2 are quite large and exhibit a rotation between the images [Table III(a) and Fig. 1]. This is due to an orbit misalignment that determines a nonnegligible baseline variation, as will be demonstrated later. For the sake of brevity, Table III reports only the shifts of tandem pairs 2 and 3. On the other hand, the following analysis will demonstrate that the tandem pairs 1 and 4 do not exhibit high correlation coefficients.

The resulting interferogram was oversampled 4 times by using the same technique, and finally, a coherent multilook (20 azimuth looks, four range looks) was executed, averaging the complex values to give the maximum likelihood estimation of the phase [15]. The selected oversampling ratio and averaging window dimensions determined the final interferogram pixels to image an almost square area on the ground (20 × 20 m^2), as it could be obtained by means of an averaging operation over a nonoversampled five azimuth pixels × one slant range pixel window.

IV. CORRELATION ANALYSIS

Several authors have showed that correlation is a significant parameter to measure the interferogram quality and the capability of applying efficiently phase unwrapping procedures [7], [16].

For each coregistered image pair, the correlation coefficient was computed as [17]

$$\gamma = \frac{|\langle P_1 P_2^* \rangle|}{\sqrt{\langle P_1^2 \rangle \langle P_2^2 \rangle}} \tag{1}$$

where P_1 and P_2 are the complex values of homologous pixels in the two images of the interferometric pair, P^* is the com-

TABLE III

SUBPIXEL RANGE AND AZIMUTH SHIFTS COMPUTED IN THE INTERFEROMETRIC PAIRS (a) 2 AND (b) 3. BOLD CELLS CONTAIN AT LEAST ONE CR

(a)

Azimuth position	Range bin 1	128	256	384	512	640	768	896	1024	1152	1280	1408	1536	1665	1792	1900
512	2,-8	4,-10	8,-2		12,-1	15,0	20,0	22,3	24,3	26,8	30,9	34,9		37,10	
1024	1,-10		7,0	8,0	11,0	16,0	20,0	21,0	22,0			33,9	37,10			
1536			7,0	8,-3	12,-1	16,1	17,0	21,1	23,2	27,2			34,9		43,10	
2048		5,-10		8,-1	11,-1	15,0	17,0	22,0	23,2		31,9	32,9		40,11	41,12	
2560	0,-8		7,-3	9,0	12,-3		16,1	23,0	25,5		31,7	34,10	34,10	38,10		
3072	-1,-9		5,-2	7,-1	13,0	14,-1	18,0	21,0		27,9	31,8			41,10	41,12	
3584	-3,-10	3,-10		4,0	13,-1	15,0	18,1							39,11		
4096	-2,-10		5,-2	9,-1	13,-1	16,1	19,1							38,11		
4608	-1,-8	2,-9	6,-1	8,-1	13,1		19,1				33,9	34,8		40,11		
5120	0,-9		5,0				16,1	19,5					35,10			
5832	0,-10	2,-2			12,1	14,3						32,10	35,11	38,10	41,10	
6144	-1,-9	4,-2									30,9	33,8	32,12	38,10	39,11	
6656	-2,-9						19,2				29,10	32,9	33,9			
7168	-4,-9		6,0	8,-1						23,9	28,10		33,10	36,10	37,11	
7680	-1,-8	1,-1	5,0				17,3		23,8			30,9	34,10	37,12	37,11	
8192	-4,-10					15,2	16,1		22,3	25,4	30,10		31,9	36,11		
8704			4,1	8,-1	12,1		19,-2	19,-1	23,9	23,4	29,11	31,10	32,10		37,11	
9000	-3,-9			8,-1			17,0	19,1	22,9	25,6	25,9	31,10	31,10		35,9	

(b)

Azimuth position	Range bin 1	128	256	384	512	640	768	896	1024	1152	1280	1408	1536	1665	1792	1900
512	5,10	6,9	6,9	6,9	9,10		9,10	10,9	10,9	11,10	11,10	13,9	13,9	14,10		
1024		6,9	6,10	7,10	7,9	8,9	8,8	9,9	9,9		11,9	13,9	13,9	13,9		
1536			7,10	6,8	7,9	8,8	6,10	8,9	10,9	12,9			13,9			
2048				7,9	7,7	6,10	6,7	9,10	10,7		12,10	10,9				
2560	5,10	5,8	7,8	6,9	8,10	8,8	9,9	9,8		12,9	12,8	12,10	13,9		12,9	
3072	7,11	6,9	5,9	7,8	8,10	8,9	8,8	10,10		11,10	12,8			16,8		
3584		5,9		7,7	8,9	8,10	9,8	9,10						13,11	13,6	
4096		6,10	7,10	7,9	8,10	8,9	9,9				12,11	11,10		14,8	15,9	
4608	8,12	5,8	6,8	7,9			9,9					16,12			12,9	
5120	6,10		5,9				9,10						13,10		14,11	
5832	5,9	5,10						11,13				11,7	11,10	13,9		
6144	5,9		8,10								11,7	12,11		13,8	14,8	
6656	5,10					7,11	9,9				11,10	12,9	12,8	14,13		
7168			8,10	9,9				10,10			12,10	13,9	12,9	14,9	15,7	
7680		5,10	6,9				9,9	10,9	11,8	11,7	12,10	13,9	13,10	13,9	14,9	
8192					7,11	11,9	10,10	10,9	10,10	13,10	12,10		12,9	14,9		
8704					10,9				10,9	10,9	11,11	12,9	12,10		14,9	
9000				8,9		10,10	9,8	10,10	9,8	11,9	11,10		12,9		16,11	

TABLE IV

NUMBER OF GCP'S USED TO COMPUTE POLYNOMIAL COEFFICIENTS AND GEOMETRIC REGISTRATION ERRORS FOR THE CONSIDERED TANDEM PAIRS

Tandem Pair	Number of GCPs	Registration errors (subpixel) rms		maximum	
		range	azimuth	range	azimuth
1	156	1	1	+4	+7
2	159	1	2	-8	-5
3	159	1	1	-4	-4
4	151	2	1	+8	-3

plex conjugate of pixel P, and $\langle\cdot\rangle$ is the expectation computed averaging the complex pixels. Fig. 2 shows the correlation map corresponding to the tandem pair 2. Large decorrelated areas exist, as expected, considering the results pointed out in the previous paragraph [shaded subsets in Table III(a)]. Low correlation regions correspond mainly to steep reliefs. Furthermore, decorrelated lakes and rivers can be easily identified. Satisfactory correlation coefficients are obtained over flat (slope ranging from 0 to 60%) vegetated (mostly cereals, forage, and pasture grass) areas. It is worth noting that the ERS radar operates in C-band (wavelength 5.6 cm), which makes decorrelation more likely with respect to longer wavelengths. The correlation maps of the other interferograms are quite similar and not reported for the sake of brevity. The computed average values are listed in Table V, where it is manifest that the tandem pairs 2 and 3 are more correlated.

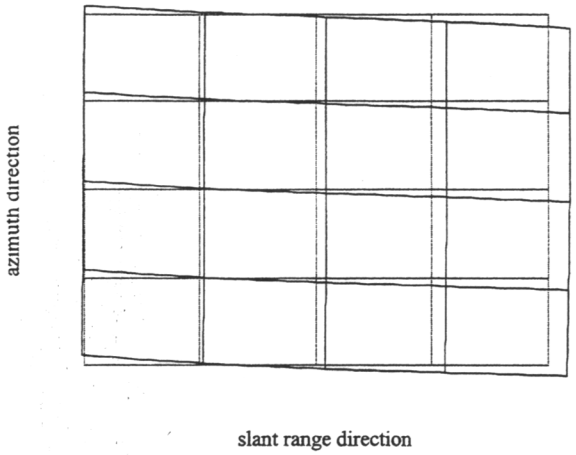

Fig. 1. Schematic of image rotation in tandem pair 2 (not in scale). Solid line ERS-1 Nov. 14, 1995, image, dashed line ERS-2 Nov. 15, 1995, image.

Fig. 2. Correlation map of tandem pair 1.

TABLE V
AVERAGE CORRELATION COEFFICIENTS

Tandem pair	Average correlation coefficient	
	whole scene	selected subset
1	0.50	0.57
2	0.54	0.62
3	0.61	0.68
4	0.46	0.56

To avoid decorrelation problems and speed the processing, we decided to limit our successive activities to a square subset (about 10×10 km^2, corresponding to 512×512 pixels, after the previously described processing), put in evidence in the lower right corner in Fig. 2, where adequate correlation coefficients were available (Table V). The selected area comprises three CR's (numbers 6, 7, and 8 in Table I) and three more bright point targets, assumed as GCP's. These reference points were exactly located also on topographic maps and

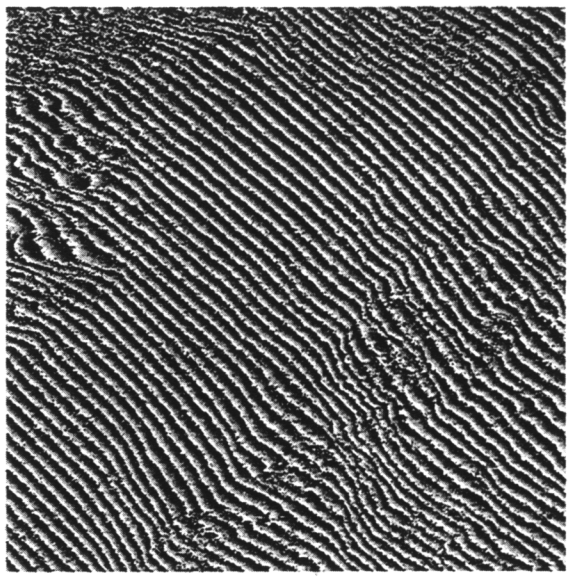

(a)

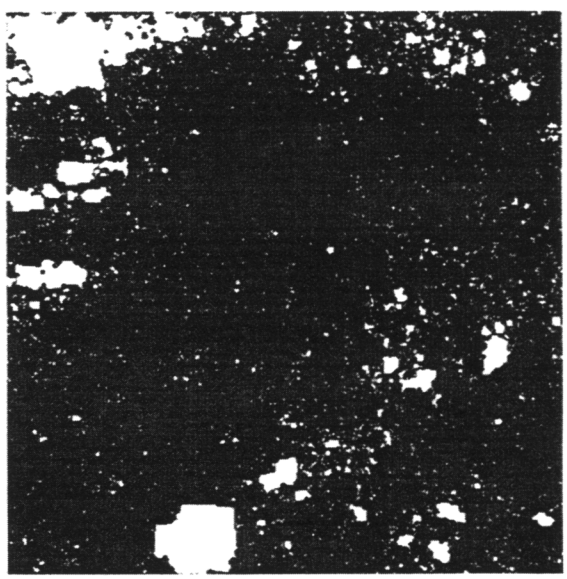

(b)

Fig. 3. (a) Interferogram of the subset extracted from tandem pair 2, and (b) the white areas correspond to subset regions cancelled by the phase unwrapping procedure after connecting the residuals.

uniformly distributed across the scene. Although the CR radiometric quality was limited and obviously the three additional GCP's were not real calibrators, the availability of reference points will be extremely useful to check the computed heights quantitatively and refine the baseline estimation, as it will be shown in the following. Finally, Figs. 3(a) and 4(a) depict the interferograms obtained from the tandem pairs 2 and 3.

In order to check our results, we selected as reference the product of the "ISAR-Interferogram Generator" software, officially distributed by ESA (Version 3.0 7/7/95). This software performs an iterative geometric registration, produces and filters the interferograms, and is also able to remove the contribution of flat earth without using orbital data. We could not compare our results to the final product of ISAR since we adopt a different strategy: after the already described geometric

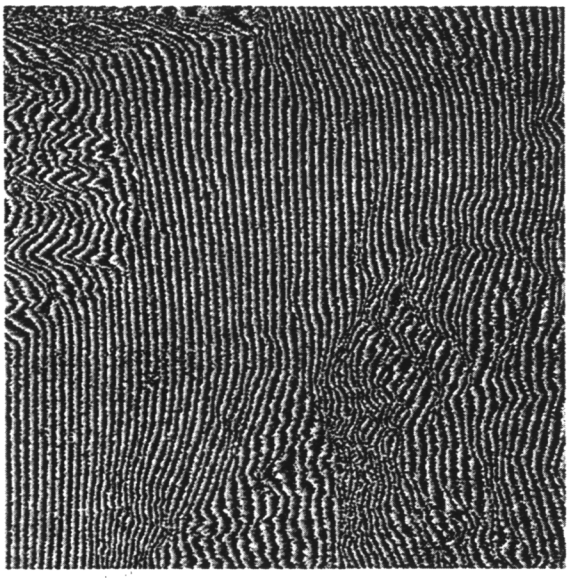

(a)

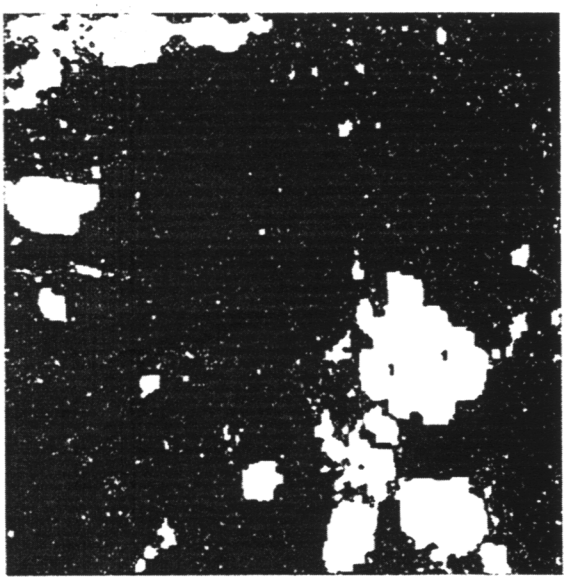

(b)

Fig. 4. Same as Fig. 2 for tandem pair 3.

registration and interferogram production, we do not operate any filtering to the interferograms, but we estimate the baseline and then unwrap the phases and compute the DEM of the area. Our procedure does not remove the contribution of flat earth from the interferogram since its effect is taken into account at the stage of DEM generation, being automatically sensitive to the computed baseline variation. For this reason, we could only compare an intermediate result, that is, the correlation of the interferometric pair after geometric registration. In particular, the ISAR product we considered was the interferometric pair after geometric registration and filtering to remove nonoverlapping parts of the range spectra of the images. Due to disk space and time limitations, we performed the comparison using only the selected subset as input. In fact, the ISAR software requires an amount of disk space much larger than the dimensions of the SLC images, which in our case were 130 MB. After geometric registration, a coherent multilook was applied to obtain the same pixel size in the complex images processed by using ISAR routines and our procedure. Finally, we computed the correlation coefficients as defined in (1), confirming the results listed in Table V.

The next processing stage is the phase unwrapping. Our procedure consists of two steps. First, to avoid error propagation, it is necessary the identification of residues, i.e., local errors in interferometric phase [18]. Then, we group them by enlarging a 2-D window according to the residue spatial distribution. The adaptive search ends when a single area contains an equal number of positive and negative residues and, consequently, it is cancelled [Figs. 3(b) and 4(b)] [19]. This procedure is performed without considering any thresholding in the local value of correlation, although, as expected, correlation is low where residues are numerous.

V. Baseline Estimation

Our procedure for baseline estimation is based on ERS-1 and ERS-2 orbital data, in particular, we used the propagated state vectors (PSV's), i.e., five satellite state vectors computed for each SLC image at approximately 2.5-s intervals and listed in the CEOS-formatted SLC header (leader file, platform position data record). The elements of the state vector are the components of the satellite position and velocity vectors with respect to a geocentric, earth-fixed, right-handed reference frame. A fourth-order polynomial is then computed for each component as a function of time. The interferometric baseline is given by the satellite separation when the antennas view the same target, that is, when the target is in the range elevation planes of both antennas. We compute the corresponding orbital times at 1/pulse repetition frequency (PRF) accuracy by using the SLC images after coarse registration. The satellite state vectors are calculated by using the polynomials, and then, the baseline components are computed. To this end, we adopt a right-handed reference frame, whose origin is coincident with one satellite position, vertical z-axis directed toward the earth center and lateral y-axis perpendicular to the plane defined by spacecraft position and velocity vectors (Fig. 5). In addition, we compute the baseline in-plane components, i.e., parallel and perpendicular to the line-of-sight (Table VI). The x-, y-, and z-components will be used as input for the procedure to compute terrain elevation, taking account of the baseline azimuth variation.

Furthermore, the baseline estimation procedure allows us to gain further insight into some aspects previously pointed out. In particular, Table III(a) and Fig. 1 put in evidence the need for an image rotation to form the interferogram. Moreover, Fig. 3(a) shows the fringes over an almost flat area not aligned to the ground track. As already mentioned, these aspects are consequent to a baseline variation [Fig. 6(a)]. In particular, the 7-m variation of baseline y-component during the 9000 lines can be related to the variation of round-trip time. With reference to Fig. 5, the slant-range difference ΔR can be computed as a function of the baseline components. Assuming $\theta = 18°$, $R_1 = 860\,000$ m, and B_x, B_y, B_z, as plotted in Fig. 6(a), it is immediate to relate the ΔR variations along the image,

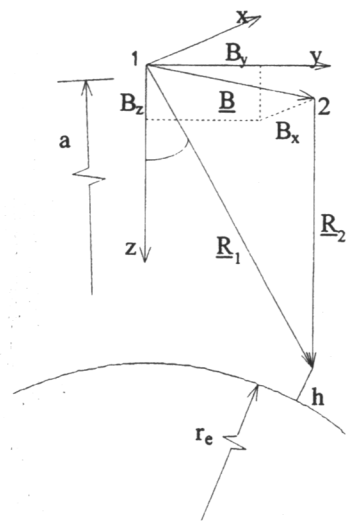

Fig. 5. Geometry of observation.

TABLE VI
BASELINE COMPONENTS COMPUTED AT SCENE CENTER

Tandem pair	Baseline components (m)				
	B_x	B_y	B_z	$B_{//}$	$B_\perp$
1	46.8	57.8	-1.6	16.3	55.4
2	74.0	-80.9	39.1	12.2	-89.0
3	-9.3	218.7	40.6	106.0	195.5
4	2.6	131.1	7.7	47.9	122.3

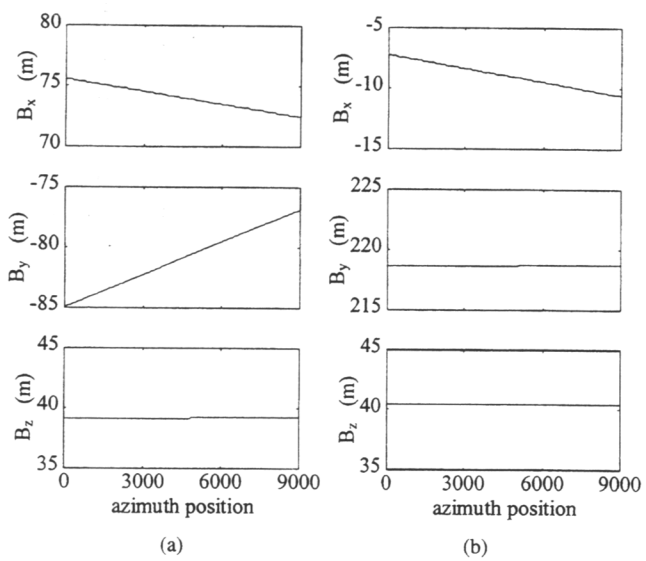

Fig. 6. Baseline components for tandem pairs (a) 2 and (b) 3.

measured in wavelength, to the 2π phase rotations over a flat area at constant range bin. In Fig. 4(a), we can measure 6.7 null lines along 500 single-look azimuth pixels, corresponding to 100 azimuth pixels in the multilook interferogram.

VI. DEM GENERATION

With reference to Fig. 5, the height (h) of each pixel above a local spherical earth (radius r_e) is given by

$$h = [(a - R_1 \cos\theta)^2 + (R_1 \sin\theta)^2]^{1/2} - r_e \qquad (2)$$

TABLE VII
HEIGHT ERRORS ON THE GCP'S AND APPLIED CORRECTIONS

Tandem pair	Preliminary DEM rms GCP height error (m)	B_y maximum correction (cm)	2π ambiguity correction (cycles)	Refined DEM rms GCP height error (m)
1	104.1	+3.0	+39	26.8
2	12.6	-1.8	-4	4.8
3	8.9	+4.4	-5	3.4
4	53.9	+8.0	+2	7.9

where a is the orbit semimajor axis. The side looking angle θ is related to the interferometric phase difference Φ as follows:

$$\Phi = \frac{2\pi}{\lambda} 2(R_1 - R_2) \cong \frac{4\pi}{\lambda}\left[(B_z \cos\theta - B_y \sin\theta) - \frac{B^2}{2R_1}\right] \qquad (3)$$

where λ is the wavelength and the slant-range difference was approximated by baseline second-order Taylor series. Of course, a GCP must be used to solve the first 2π ambiguity after phase unwrapping.

As shown in [13], one of the most significant height error sources is the baseline uncertainty, which in our procedure is consequent to an inaccurate estimation of satellite positions. In particular, a constant error in baseline estimation causes an incorrect solution of the 2π ambiguity and, consequently, an error propagation in across-track direction, while an erroneous baseline time derivative introduces a ramp in the along-track direction. Several authors proposed original techniques to remove the above inaccuracies. As an example, in [2], the interferometric phase was modified by means of a constant and a linear term computed by using tie points. In [20], a method was introduced to compute a phase constant, an azimuth convergence factor, and two constant baseline components for precise baseline estimation by using tie points well distributed across the scene. Our procedure is aimed at the improvement of the 2π ambiguity solution and the refinement of the estimation of one baseline time-varying component by using the GCP heights.

As shown by (3), the most relevant contribution is given by the B_z and B_y inaccuracies, whereas the B_x component is less important. Furthermore, the computed B_z variations are negligible with respect to the B_y ones [Fig. 6(a) and (b)]. Therefore, our strategy was based on the minimization of the GCP height errors in a least-squares sense, by adding a linear term to B_y in azimuth direction and a constant term to the 2π cycles. Table VII shows the results obtained before and after the application of the procedure. The root mean square (rms) error was computed using only the four GCP's not included in the regions cancelled by the phase unwrapping procedure. In the four considered cases, the procedure worked properly, requiring limited corrections. In particular, in the tandem pairs 2 and 3, we obtained results comparable to the ones presented in [2].

Then, we performed a comparison of the whole area, obtaining a rms difference of 18.7 m in the best case [Fig. 7(a) and (b)]. This less effective result is obviously due to temporal decorrelation of extended areas with respect to point targets, as pointed out in [16], where an rms height error of 2.7 m

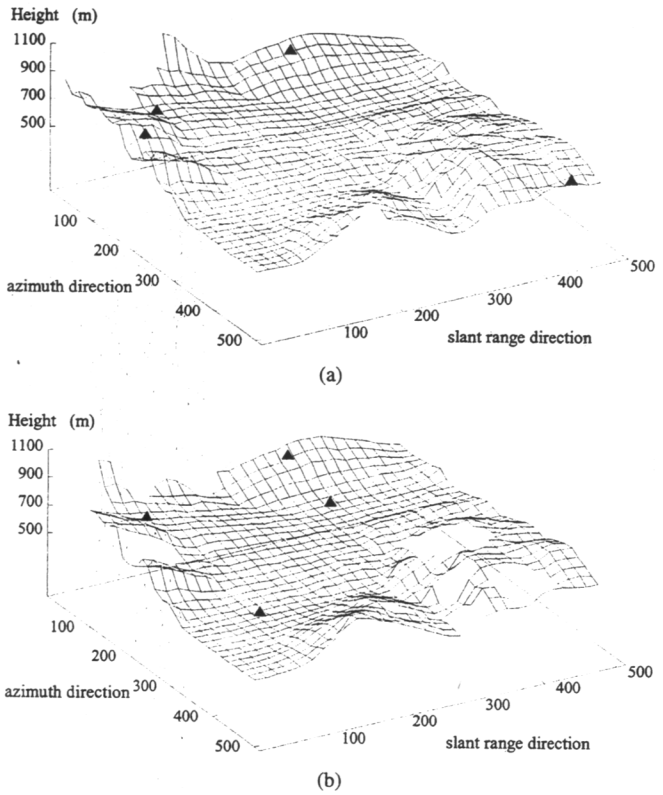

Fig. 7. DEM's of the interferometric pairs (a) 2 and (b) 3. Triangles show the available GCP's.

TABLE VIII
COMPARISON OF THE DEM'S OBTAINED FROM THE AVAILABLE TANDEM PAIRS

Tandem pairs		Rms height difference (m)	Time separation between tandem passes (days)
1	2	30.5	105
1	3	31.9	210
1	4	40.8	245
2	3	18.7	105
2	4	33.8	140
3	4	25.6	35

TABLE IX
SELECTED INTERFEROMETRIC PAIRS AND CORRELATION COEFFICIENTS

Interferometric pair				Baseline components (m)					Temporal baseline (days)	Average correlation coefficient
sat.	date	sat.	date	B_x	B_y	B_z	$B_{//}$	$B_\perp$		
ERS-1	01 Aug 95	ERS-1	27 Feb 96	55.4	-84.2	-77.2	-99.4	-56.2	210	0.39
ERS-1	01 Aug 95	ERS-2	28 Feb 96	46.1	134.5	-36.8	6.6	139.3	211	0.38
ERS-1	01 Aug 95	ERS-1	02 Apr 96	5.5	-105.4	-35.7	-66.5	89.2	245	0.24
ERS-1	01 Aug 95	ERS-2	03 Apr 96	8.2	25.7	-27.9	-18.6	33.1	246	0.25
ERS-2	02 Aug 95	ERS-1	27 Feb 96	4.1	-142.1	-75.5	-115.7	-111.8	209	0.24
ERS-2	02 Aug 95	ERS-2	28 Feb 96	-5.3	76.6	-35.5	-9.6	83.7	210	0.24
ERS-2	02 Aug 95	ERS-1	02 Apr 96	-41.4	-163.2	-34.0	-82.7	-144.7	244	0.23
ERS-2	02 Aug 95	ERS-2	03 Apr 96	-38.7	-32.1	-26.2	-34.9	-22.5	245	0.25
ERS-1	27 Feb 96	ERS-1	02 Apr 96	-44.6	-21.1	41.5	33.0	32.9	35	0.31
ERS-1	27 Feb 96	ERS-2	03 Apr 96	-42.0	109.9	49.3	80.8	89.3	36	0.30
ERS-2	28 Feb 96	ERS-1	02 Apr 96	35.7	239.8	-1.1	73.1	228.4	34	0.30
ERS-2	28 Feb 96	ERS-2	03 Apr 96	-33.1	-108.9	8.8	-25.2	-106.2	35	0.24

was attained on a comparably large area when correlation was instead greater than 0.8. For the sake of clarity, in Fig. 7 16 × 16 DEM pixels were averaged to plot a single height point. Fig. 7 shows also the areas cancelled by the unwrapping procedure.

The procedure for DEM production applied to the tandem pairs 1 and 4 required additional processing steps. Since the average correlation coefficients were 0.50 on the whole scene and only 0.57 on the selected subset in the best case, the phase unwrapping procedure identified a large number of residuals and cancelled large areas, making impossible an adequate DEM production. To avoid this problem, an additional coherent multilook was applied (two azimuth looks and two range looks). As a result, larger rms height errors on the GCP's were obtained (26.8 and 7.9 m) with respect to the tandem pairs 2 and 3 (Table VII). With reference to the DEM's, Table VIII lists the rms height differences between all available DEM pairs. As expected, the tandem pairs with low correlation present large variances.

VII. DIFFERENTIAL INTERFEROMETRY

To make possible differential interferometry, it is necessary to identify a third coverage offering high correlation coefficients and satisfactory baseline with at least one of a tandem pair, provided that the tandem interferogram was satisfactory. To this end, first of all, we selected the tandem and nontandem pairs with an adequate baseline. Unfortunately, we had to exclude the pair 2, since it never met the baseline requirement, as demonstrated by the Interferometric Orbit Listings provided by ESA/ESRIN. Table IX reports the considered pairs and the computed baselines. At this stage, we evaluated the correlation coefficients but were unable to identify any satisfactory area, even considering relatively small subsets, in spite of the very large data set. Consequently, it was not possible to apply phase unwrapping and produce differential interferograms, apart from very small and irregular areas, where neither GCP's nor geographic references were found. For the sake of completeness, we computed the correlation coefficients over small subsets after registration performed by means of ISAR routines, obtaining comparable results.

VIII. CONCLUSIONS AND FUTURE ACTIVITIES

This paper presented an end-to-end procedure for DEM generation using ERS-1/ERS-2 tandem data. The method was applied to a test area located in southern Italy, where nine CR's were deployed and four tandem pairs were available. A method for baseline estimation refinement by using the GCP heights was presented. Furthermore, the point target height measurement accuracy was validated on the adopted GCP's, obtaining satisfactory rms errors of the order of 4 m in the best cases (November 1995 and February 1996 tandem pairs), values comparable to the results presented by other authors in different conditions [2]. The worst value was 26.8 m, obtained using as input the August 1995 tandem pair. These results put in evidence the product instability consequent to unpredictable time decorrelation. With reference to extended targets, the DEM's exhibited significant variances, also in the presence of high correlation coefficients. Consequently, we think that it is unlikely to obtain high-resolution and high-accuracy DEM's

(i.e., that meet map accuracy standards) on a global scale by means of repeat-track interferometry. On this issue, the future Shuttle Radar Topography Mission will certainly play an outstanding role, thanks to the simultaneous use of transmitting and receiving antennas. Although boom oscillations, antenna pointing requirements, and baseline measurement techniques must be carefully studied in this case. On the other hand, ERS tandem data allow low-resolution, global-scale DEM's to be accomplished, provided that adequate baseline estimation accuracy is available. This paper reported also on the impossibility of performing differential interferometry on the test area by using at least one nontandem pair. In spite of the availability of six passes, time decorrelation caused correlation coefficient values always less than 0.40.

Our future research activity will deal with high geometric precision and phase-preserving processing of SAR raw data by using orbital and attitude inputs for interferometric applications. Our main targets will be image quality and correlation improvements and DEM geocoding. In particular, considering the difficulties experienced in CR detection, we will improve the deployment campaign (e.g., CR's embedded in absorbing background and forming a clear geometrical pattern) and apply high-order focusing techniques (e.g., phase gradient autofocus) to increase the detectability of these man-made point targets. Furthermore, thanks to the availability of several tandem pairs, we will adopt multibaseline techniques to integrate output DEM's. To this end, we have submitted the proposal "Use of ERS-1/ERS-2 Tandem Data for Earthquakes Prediction in Tectonic Active Areas" (ERS-1/2 experiment code AOT.I302) to the ESA Announcement of Opportunity for the Scientific Exploitation of the ERS Tandem Mission.

REFERENCES

[1] L. C. Graham, "Synthetic interferometer radar for topographic mapping," *Proc. IEEE,* vol. 62, pp. 763–768, June 1974.

[2] H. A. Zebker, C. L. Werner, P. Rosen, and S. Hensley, "Accuracy of topographic maps derived from ERS-1 interferometric radar," *IEEE Trans. Geosci. Remote Sensing,* vol. 32, pp. 823–836, July 1994.

[3] A. K. Gabriel, R. M. Goldstein, and H. A. Zebker, "Mapping small elevation changes over large areas: Differential radar interferometry," *J. Geophys. Res.,* vol. 94, no. B7, pp. 9183–9191, 1989.

[4] G. Duchossois and P. Martin, "ERS-1 and ERS-2 tandem operations," *ESA Bull.,* no. 83, pp. 54–60, 1995.

[5] Topsat Working Group, "Scientific requirements a future space global topography mission," Italian Space Agency, Roma, Italy, Rep. Contract ASI-92-RS-S2, 1994, p. 85.

[6] F. Li and R. M. Goldstein, "Studies of multi-baseline spaceborne interferometric synthetic aperture radars," *IEEE Trans. Geosci. Remote Sensing,* vol. 28, pp. 88–97, Jan. 1990.

[7] H. A. Zebker and J. Villasenor, "Decorrelation in interferometric radar echoes," *IEEE Trans. Geosci. Remote Sensing,* vol. 30, pp. 950–959, Sept. 1992.

[8] CORISTA, "Earthquakes prediction in tectonic active areas using space techniques," Commission Eur. Communities, Napoli, Italy, Tech. Rep., Contract EV5V-CT94-0461, 1995–1996.

[9] L. Polidori and P. Armand, "On the use of SAR image simulation for the validation of topographic mapping techniques," *EARSeL Adv. Remote Sensing,* vol. 4, no. 2, pp. 40–48, 1995.

[10] S. Bruzzi, J. P. Guignard, and T. Pike, "Quality assessment of remote-sensing data: The SAR case," *ESA J.,* vol. 6, no. 3, pp. 371–281, 1982.

[11] A. Moccia, S. Vetrella, and S. Ponte, "Passive and active calibrators characterization by using reference reflectors," *IEEE Trans. Geosci. Remote Sensing,* vol. 32, pp. 715–721, May 1994.

[12] JPL SIR-C Team, DLR NE-HF X-SAR Team, and I-PAF X-SAR Team, "Data products and image quality specifications for the SIR-C/X-SAR mission," Jet Propul. Lab., Pasadena, CA, Doc. D-7193, 1990.

[13] A. Moccia, S. Esposito, and M. D'Errico, "Height measurement accuracy of ERS-1 SAR interferometry," *EARSeL Adv. Remote Sensing,* vol. 3, no. 1, pp. 94–108, 1994.

[14] I. Dowman, "The geometry of SAR images for geocoding and stereo applications," *Int. J. Remote Sensing,* vol. 13, no. 9, pp. 1609–1617, 1992.

[15] C. L. Werner, R. M. Goldstein, P. Rosen, and H. A. Zebker, "Techniques and applications of SAR interferometry for ERS-1: Topographic mapping, slope measurement and change detection," in *Proc. 1st Workshop ERS-1 Fringes Working Group,* ESA ESRIN, Frascati, Italy, 1992, p. 11.

[16] D. Small, C. L. Werner, and D. Nüesch, "Geocoding and validation of ERS-1 InSAR-derived digital elevation models," *EARSeL Adv. Remote Sensing,* vol. 4, no. 2, pp. 26–39, 1995.

[17] E. Rodriguez and J. M. Martin, "Theory and design of interferometric synthetic aperture radars," *Proc. Inst. Elect. Eng.,* vol. 139, no. 2, pp. 147–159, 1992.

[18] R. M. Goldstein, H. A. Zebker, and C. L. Werner, "Satellite radar interferometry: Two-dimensional phase unwrapping," *Radio Sci.,* vol. 23, no. 4, pp. 713–720, 1988.

[19] G. Alberti, S. Esposito, and S. Vetrella, "The Vesuvius DEM: A test case for the TOPSAR system," in *Proc. MAC Europe'91 Final Results Workshop,* Lenggries, Germany, Oct. 4–6, 1994, pp. 49–55.

[20] D. Small, C. L. Werner, and D. Nüesch, "Baseline modeling for ERS-1 SAR interferometry," in *Proc. Int. Geosci. Remote Sens. Symp.,* Tokyo, Japan, Aug. 18–21, 1993, pp. 1204–1206.

Giancarlo Rufino received the Doctoral degree in aeronautical engineering in 1994 from the University of Naples, Naples, Italy. He is currently pursuing the Ph.D. degree in aerospace engineering from the University of Naples.

He is developing his research activity on spaceborne systems for SAR interferometry, under the sponsorship of the European Community.

Antonio Moccia has been a Professor of Aerospace Servosystems at the Faculty of Engineering, Naples, Italy, since 1990. His research activities deal with aerospace high-resolution remote-sensing system design and data processing as well as space systems dynamics and control. In these areas, he has been a member of national and international working groups (ASI, NASA, ESA) and Principal or Co-Investigator of several research programs. In particular, since 1975, he has held several grants and research contracts from the National Research Council, the University of Naples, the Italian Space Agency, Alenia Spazio, and Telespazaio.

Salvatore Esposito received the degree in electronic engineering in 1992 from the University of Naples, Naples, Italy.

He has been with Consorzio di Ricerca su Sistemi di Telesensori Avanzati (CORISTA), a consortium for the research on advanced remote-sensing systems, Naples, since 1992, where he has been Co-Investigator of several national and international programs of research (ASI, NASA, CEC) in the field of interferometric SAR data processing. Since 1995, he has been involved in several international programs (ESA) for the design of new conception remote-sensing systems.